文章编号：1001-9014(2025)03-0405-07

DOI:10.11972/j.issn.1001-9014.2025.03.010

Design and preparation of LWDM AWG for 1.6Tbps and above data center

HUANG Song[1,3], CUI Peng-Wei[1,3], WANG Yue[1*], WANG Liang-Liang[1], ZHANG Jia-Shun[1], MA Jun-Chi[1,3], ZHANG Chun-Xue[1,3], GUO Li-Yong[1,3], YANG Han-Ming[1,3], WU Yuan-Da[1,2,3], AN Jun-Ming[1,2,3], SONG Ze-Guo[4]

(1. Key Laboratory of Optoelectronic Materials and Devices, Institute of Semiconductors, Chinese Academy of Sciences, Beijing 100083, China;
2. Center of Materials Science and Optoelectronics Engineering, University of Chinese Academy of Sciences, Beijing 100049, China;
3. College of Materials Science and Opto-Electronic Technology, University of Chinese Academy of Sciences, Beijing 100049, China;
4. Wuxi Institute of Interconnect Technology, Co., Ltd Wuxi 214101, China)

Abstract: A 16-channel arrayed waveguide grating (AWG) with an 800 GHz channel spacing in the O-band has been developed and fabricated based on silica planar lightwave circuit (PLC) technology. By extending the wavelength allocation from 8 channels to 16 channels as specified in IEEE 802.3bs, we increased the number of channels and boosted transmission capacity to meet the 1.6 Tbps and higher-speed signal transmission requirements for future data centers. Through optimizing the AWG structure, it has achieved insertion loss (IL) better than -1.61 dB, loss uniformity below 0.35 dB, polarization-dependent loss (PDL) below 0.35 dB, adjacent channel crosstalk under -20.05 dB, ripple less than 0.75 dB, center wavelength offset under 0.22 nm and 1 dB bandwidth exceeding 2.88 nm. The AWG has been successfully measured to transmit 53 Gbaud 4-level pulse amplitude modulation (PAM4) signal per channel and the total transmission speed can reach 1.6 Tbps and above.

Key words: local area network wavelength division multiplexing (LWDM), arrayed waveguide grating (AWG), O-band, silica, planar lightwave circuit (PLC)

1.6Tbps 以上速率数据中心 LWDM AWG 的设计和制备

黄 淞[1,3], 崔鹏伟[1,3], 王 玥[1*], 王亮亮[1], 张家顺[1], 马骏驰[1,3], 张春雪[1,3], 郭利勇[1,3], 杨涵茗[1,3], 吴远大[1,2,3], 安俊明[1,2,3], 宋泽国[4]

(1. 中国科学院半导体研究所光电子材料与器件重点实验室,北京 100083;
2. 中国科学院大学材料科学与光电工程中心,北京 100049;
3. 中国科学院大学材料科学与光电技术学院,北京 100049;
4. 无锡芯光互连技术研究院,江苏 无锡 214101)

摘要:采用二氧化硅平面光波回路(PLC)技术,设计并制备了 O 波段、通道间距 800 GHz 的 16 通道阵列波导光栅(AWG)。将波长分配从 IEEE 802.3bs 规定的 8 个通道扩展到 16 个通道,增加了通道数量并提高了传输容量,以满足未来数据中心对 1.6 Tbps 及更高速信号传输的要求。通过优化 AWG 结构,使其插入损耗优于 -1.61 dB,插损均匀性低于 0.35 dB,偏振相关损耗(PDL)低于 0.35 dB,相邻信道串扰低于 -20.05 dB,纹波小于 0.75 dB,中心波长偏差低于 0.22 nm,1 dB 带宽超过 2.88 nm。同时验证了该 AWG 可以传输每通道 53.125 Gbaud 的 4 级脉冲幅度调制(PAM4)信号,总传输速率可达 1.6 Tbps 以上。

Received date: 2024-11-08, **revised date**: 2024-12-05 **收稿日期**:2024-11-08,**修回日期**:2024-12-05

Foundation items: Supported by National Key R&D Program of China (2021YFB2800201).; the Strategic Priority Research Program of Chinese Academy of Sciences (XDB43000000)

Biography: HUANG, Song (2000—), male, Shandong, China, Master, Research field is optoelectronic materials and devices, E-mail: huangsong@semi.ac.cn

[*] **Corresponding author**: E-mail: wy1022@semi.ac.cn

关 键 词:局域网波分复用(LWDM);阵列波导光栅(AWG);O波段;二氧化硅;平面光波回路(PLC)
中图分类号:TN256 文献标识码:A

Introduction

The surge in network-intensive activities such as cloud computing, artificial intelligence, and live streaming has led to a substantial increase in network data traffic. This rapid growth in communication requirements has driven advancements in high-speed optical network technologies. Optical interconnects, recognized for their high speed, large bandwidth, low latency, and reduced power consumption, are increasingly substituting traditional electrical interconnects for extensive data transmission, exchange, and processing. wavelength division multiplexing (WDM) technology plays a crucial role in optical interconnects by addressing the bandwidth challenges associated with growing communication traffic [1-3]. Devices for wavelength multiplexing and demultiplexing, which combine and separate multiple signals, are vital to WDM technology. Among these devices, arrayed waveguide gratings (AWGs) [4-5] are widely utilized in optical interconnects within data centers due to their small size, large number of channels, high level of integration and ease of mass production.

Silica-based AWG offers low insertion loss, low crosstalk, high uniformity, low cost, and ease of integration [6-8]. Lei Liu et al. [9] showcased the integration of a 4-channel coarse wavelength division multiplexing (CWDM) AWG with photodiodes (PDs) and transimpedance amplifiers (TIAs) to develop a receiver optical subassembly (ROSA) that supports the transmission of 4×25 Gbaud 4-level pulse amplitude modulation (PAM4) signals. Seok-Jun Yun et al. [10] presented a compact 4×80 Gbps transmitter-receiver optical sub-assembly (TROSA) module, employing a 4-channel AWG as both a multiplexer in the transmitter and a demultiplexer in the receiver. Cui Pengwei et al. [11] described the integration of an 8-channel local area network wavelength division multiplexing (LWDM) AWG with PD arrays, TIA arrays, and a flexible printed circuit (FPC) to create an 8×50 Gbps ROSA for use in data centers. Currently, single-channel transmission speeds can reach up to 200 Gbps [12-13]. Increasing the number of wavelength channels and enhancing the rates for single channels are key to boosting transmission capacity, which is essential for the development of advanced large-scale communication systems.

In this study, we designed and fabricated a 16-channel silica-based AWG featuring low transmission loss and channel spacing of 800 GHz, suitable for large-scale wavelength multiplexing and demultiplexing in the O-band under LWDM. By analyzing the optical transmission principles of AWG, we performed simulations to fine-tune the structural parameters of the AWG. We introduced a periodically varying grating structure in the input waveguide to minimize insertion loss (IL), improve the uniformity of the transmission spectrum, and reduce polarization-dependent loss (PDL). Consequently, we achieved an insertion loss better than -1.61 dB, PDL under 0.35 dB, and loss uniformity below 0.35 dB. Additionally, we transitioned the output waveguide from a single-mode to a multimode design to achieve a more uniform output and flat-top spectrum. The 1 dB bandwidth exceeds 2.88 nm, adjacent channel crosstalk is below -20.05 dB, and the center wavelength offset is under 0.22 nm. This AWG chip supports a single-channel transmission rate of 100 Gbps, fulfilling the requirements for 1.6 Tbps optical modules in data centers. With ongoing improvements in single-channel rates, it is anticipated to reach transmission rates of 3.2 Tbps and above in the future [14].

1 Design and Fabrication

Fig. 1 shows the schematic diagram of the AWG structure, which consists of input waveguides, an input slab waveguide, arrayed waveguides, an output slab waveguide, and output waveguides. The input and output slab waveguides are configured in a Rowland circle arrangement. As a demultiplexer, optical signals with multiple wavelengths are introduced into the slab waveguide via input waveguides separated by Δx_i, where they experience diffraction. After passing through the arrayed waveguide region with a spacing of d, the signals are separated and enter the output waveguides spaced by Δx_0, completing the wavelength demultiplexing process. The AWG′s output wavelength specifications are designed according to the IEEE 802.3bs standard, which specifies that the channel spacing for an 8-channel AWG should be 800 GHz. Based on this standard, we extended the AWG to have 16 output channels, with output wavelengths ranging from 1 269.23 nm to 1 337.17 nm, effectively covering the O-band communication range. The output wavelengths for the 16 channels are as follows: 1 269.23 nm, 1 273.54 nm, 1 277.89 nm, 1 282.26 nm, 1 286.66 nm, 1 291.10 nm, 1 295.56 nm, 13 00.05 nm, 1 304.58 nm, 1 309.14 nm, 1 313.73 nm, 1 318.35 nm, 1 323.00 nm, 1 327.69 nm, 1 332.41 nm, and 1 337.17 nm. This expansion significantly increases transmission capacity.

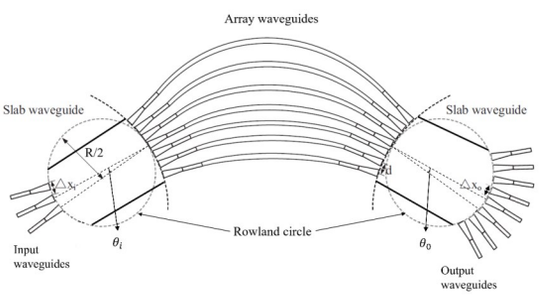

Fig. 1 The schematic structure of the AWG.
图1 AWG的结构示意图

The AWG is constructed on a silica-based platform, which provides low loss, low cost, compatibility with single-mode fibers, excellent thermal stability, and polarization insensitivity. In order to reduce the size of the AWG chip, the silica material system based on ultra-high refractive index difference of 2% chosen to build the waveguide structure. The refractive index of upper, lower cladding layer and core layer is 1.447, 1.447, and 1.477, respectively, and the height of core layer is 4μm. Simulations are performed to investigate how the effective refractive index of the waveguide core layer varies with waveguide width, using two wavelengths—1 260 nm and 1 360 nm—to cover the O-band range. The results of these simulations, shown in Fig. 2, indicate that for single-mode operation, the waveguide width must be kept below 4 μm. As a result, the input waveguide width is set to 4 μm.

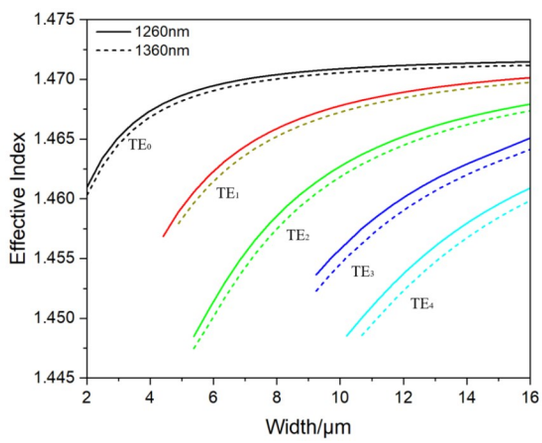

Fig. 2　Variation of mode effective refractive index with waveguide width
图2　模式有效折射率随波导宽度的变化

The transmission of light from the input Rowland circle to the output waveguide in the AWG satisfies the grating equation:

$$n_s d \sin\theta_i + n_s d \sin\theta_0 + n_c \Delta L = m\lambda \quad , \quad (1)$$

When light is transmitted from the central input waveguide to the central output waveguide, the input angle θ_i and output angle θ_0 are zero, equation (1) can be simplified to equation (2):

$$n_C \Delta L = m\lambda_0 \quad , \quad (2)$$

$$\Delta\lambda = \frac{\Delta x_0}{R}\frac{n_s d}{m}\left(\frac{n_g}{n_c}\right)^{-1} \quad , \quad (3)$$

$$FSR = \frac{\lambda_0}{m}\left(\frac{n_g}{n_c}\right)^{-1} \quad , \quad (4)$$

In the equation, θ_0 represents the angle between the central waveguide and the output waveguide, while n_s and n_c denote the effective refractive indices of the slab waveguide and the arrayed waveguide, respectively. The variable d stands for the distance between adjacent arrayed waveguides, ΔL indicates the length difference between these waveguides, and m denotes the diffraction order. The symbol λ represents the wavelength of the incoming light, λ_0 is the central wavelength, Δx_0 refers to the spacing between adjacent output waveguides, n_g is the group index, and R signifies the radius of the rowland circle. In order to obtain lower insertion loss and less crosstalk in the spectra of neighboring diffraction levels, and to ensure that the device size is appropriate, the FSR is chosen to be 127.86 nm, and then according to Eqs. (2) and (4), we can obtain that the ΔL is 8.936 nm and m is 10.

Simulation by the three-dimensional beam propagation method (3D-BPM) determines how the coupling loss varies with the spacing between single-mode waveguides, each extending 3000 μm in parallel. Figure 3 illustrates that strong optical coupling occurs between the waveguides when the spacing is set to 6 μm. As the spacing increases to 8 μm, the optical power coupled into the adjacent waveguides decreases significantly. To ensure low coupling power while reducing the size of the chip, a final choice of 7 μm is made for input waveguide spacing (Δx_i) and arrayed waveguide spacing(d).

The optical field of an individual arrayed waveguide displays a Gaussian profile [15]. Additionally, to collect diffracted light as much as possible and reduce transmission loss caused by mode mismatch at the junction between the slab waveguide and the arrayed waveguide, a tapered waveguide structure is introduced. The parabolic tapered structure is considered a better choice for reducing crosstalk and ensuring efficient mode conversion [16]. The parabolic tapered waveguide structure and transmission field are shown in Fig. 4. To minimize transmission loss, the waveguide width is gradually increased from 4 μm to 6 μm over a length of 50 μm using a parabolic-shaped variation. Additionally, to avoid additional crosstalk and ensure dense arrangement of arrayed waveguides, a 1-μm gap is left between adjacent arrayed waveguides.

To achieve a flattened spectrum at the output end, we widened the output waveguide to a multimode waveguide. When light is focused and coupled into the output waveguide through the output slab, higher-order modes are excited. The interference of multiple modes results in a flattened spectral output. The simulated spectra with different output waveguide widths are shown in Fig. 5 (a), and it can be noticed that the flatness of the spectra improves as the output waveguide width increases. Considering both the AWG size and spectral flatness, we selected an output waveguide width of 11 μm. Table 1 lists the 1 dB bandwidth of the output spectrum for different output waveguide widths.

Additionally, simulation is performed to assess the influence of multimode waveguide spacing on crosstalk between adjacent waveguides, as depicted in Fig. 5(b). It is evident that when the multimode waveguide spacing is 14 μm, minimal coupling occurs between adjacent waveguides. Therefore, the spacing for the output waveguides is ultimately chosen as 14 μm.

In determining the other parameters, the wavelength spacing between adjacent channels is approximated to be 4.56 nm, but the channels are divided by equal

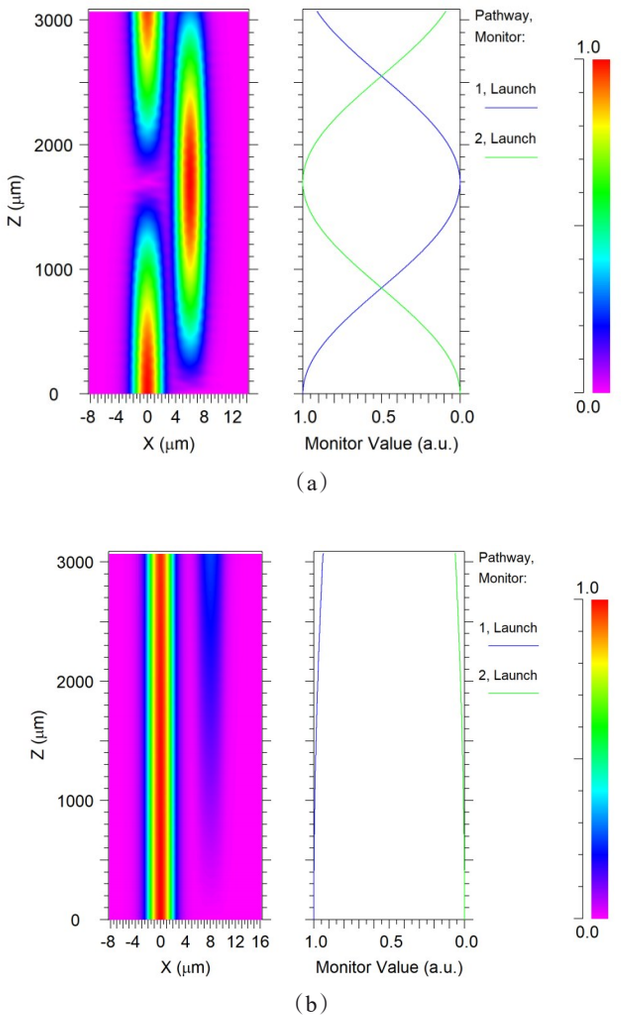

Fig. 3 (a) Simulated mode field propagation at 6 μm spacing; (b) Simulated mode field propagation at 8 μm spacing
图三 (a)6 μm间距时的模拟模场传播;(b)8 μm间距时的模拟模场传播

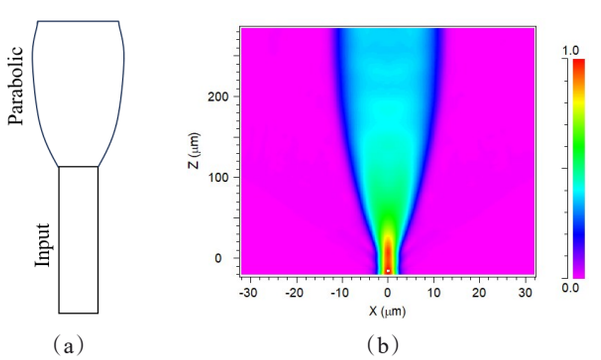

Fig. 4 (a)The top view of a parabolic taper; (b) Parabolic tapered waveguide transmission field
图4 (a)抛物线型锥形波导的俯视图;(b)抛物线型锥形波导的传输模场

frequency intervals, and the corresponding wavelength intervals are inconsistent, so in order to ensure that the

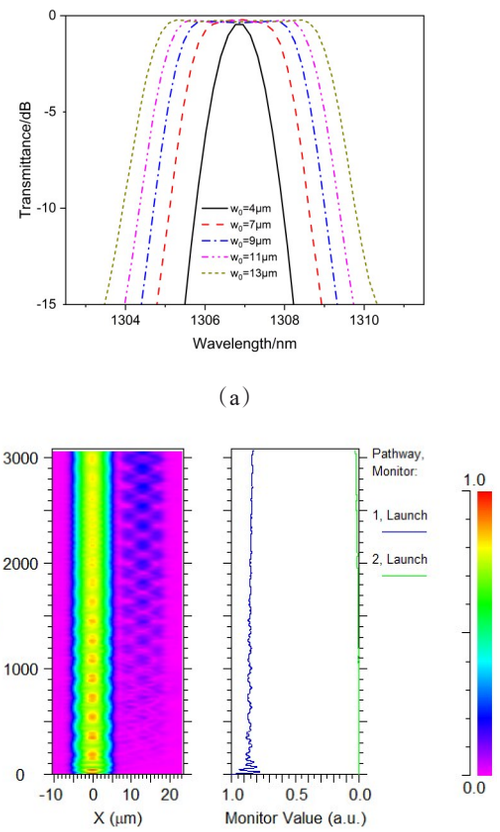

Fig. 5 (a)Spectra corresponding to different output waveguide widths;(b) Simulated mode field propagation at 14 μm spacing
图5 (a)不同输出波导宽度对应的光谱曲线;(b)14 μm间距下的模拟模式场传输

Table 1 : The simulated 1 dB bandwidth at different output waveguide widths.
表1 不同输出波导宽度下模拟的1 dB带宽

Width/μm	1 dB bandwidth/nm
4	0.56
7	1.96
9	2.69
11	3.29
13	3.94

channels are all spaced at 800 GHz, the center wavelength needs to be realigned. According to Equation (3), when other parameters are fixed, $\Delta\lambda$ is directly proportional to the spacing between output waveguides Δx_0. Therefore, the ratio $\Delta\lambda/\Delta x_0$ remains constant. Hence, it is essential to adjust Δx_0 according to the actual wavelength spacing between adjacent channels to achieve precise alignment of the center wavelengths for each output channel. The corrected output waveguide spacing δx can be determined using the relationship $\delta x = \frac{\Delta x_0}{\Delta\lambda}\cdot\delta\lambda$. At the outset of the design, the wavelength

spacing corresponding to a channel spacing of 14 μm is 4.56 nm. The corrected output waveguide spacing δx is listed in Table 2. Fig. 6 illustrates the configuration of a 16-channel silica-based AWG with an output pitch of 250 μm.

Table 2　Corrected output waveguide spacing
表二　修正后的输出波导间距

Adjacent channels	δλ(nm)	δx(nm)
1–2	4.31	13.88
2–3	4.34	13.98
3–4	4.37	14.07
4–5	4.40	14.17
5–6	4.43	14.27
6–7	4.46	14.37
7–8	4.49	14.47
8–9	4.53	14.57
9–10	4.56	14.67
10–11	4.59	14.77
11–12	4.62	14.87
12–13	4.65	14.98
13–14	4.69	15.09
14–15	4.72	15.19
15–16	4.75	15.30

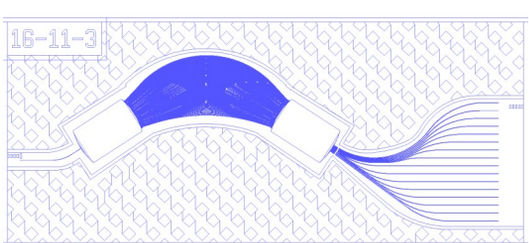

Fig. 6　The schematic of 16-channel AWG
图6　16通道AWG的版图示意图

2　Fabrication, measurements and discussions

The AWG is manufactured on a 6 inch quartz substrate wafer, bypassing the traditional method of thermally oxidizing a 15-μm thick SiO_2 lower-cladding layer on a silicon substrate. The fabrication process, depicted in Fig. 7, involves directly depositing approximately 4 μm of GeO_2-SiO_2 core layer onto a quartz-based SiO_2 substrate using plasma enhanced chemical vapor deposition (PECVD). By adjusting the germanium doping levels, we achieve a high refractive index difference of 2 % between the core and cladding layers. A 1 μm thick polysilicon layer is then applied as a hard mask using low pressure chemical vapor deposition (LPCVD). The SiO_2 waveguides are formed by photolithography and inductively coupled plasma (ICP) dry etching. Subsequently, boro-phospho-silicate glass (BPSG) is deposited as the upper cladding, employing PECVD technique. Then, the wafer is sliced to chips. To reduce back reflection losses from end-face mirror reflections, the waveguide end faces are polished at an 8° angle. Finally, the input and output waveguides of the AWG chip are coupled with fiber arrays (FA) for testing. The completed AWG is shown in Fig. 8.

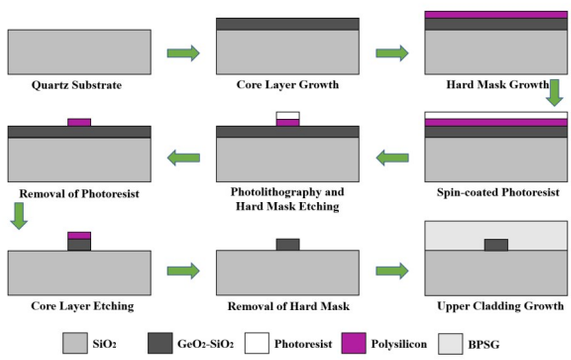

Fig. 7　The schematic diagram of the 16-channel AWG fabrication process
图7　16通道AWG的制造工艺流程图

Utilizing the experimental setup shown in Fig. 9 (a), we perform spectral testing on the AWG. An O-band tunable laser serves as the input source and a polarization controller is used to adjust the light's polarization state. Following this adjustment, an optical power meter is employed to accurately measure and record the optical power output from each channel over the entire spectral range. The measured spectral response is depicted in Fig. 9(b).

Fig. 10(a) shows the insertion loss. The insertion loss (IL) for each channel at standard wavelengths ranges between -1.26 dB and -1.61 dB, loss uniformity is below 0.35 dB, indicating good uniformity. Fig. 10(b) depicts the polarization-dependent loss for each channel. The polarization-dependent loss (PDL) stays below 0.35 dB near the center wavelength of each channel, showing low sensitivity to polarization. Fig. 10(c) depicts the crosstalk of each channel. The adjacent crosstalk (AX), non-adjacent crosstalk (NX) and total crosstalk (TX) are more than 20.05 dB, 23.37 dB and 12.58 dB, respectively. The crosstalk can be further optimized by increasing the number of array waveguides, achieving effective wavelength separation. Fig. 10(d) depicts the ripple for each channel. The worst ripple of all channels is less than 0.75 dB. Fig. 10(e) shows the offset between the center wavelength and standard wavelength, the largest center wavelength offset being 0.22 nm for any output channel. Fig. 10(f) shows bandwidth characteristics of the AWG. For all channels, the 1 dB bandwidth is greater than 2.88 nm, and the minimum 3 dB bandwidth is 3.52 nm, demonstrating a flat spectral distribution. The smaller ripple and larger bandwidth guarantee the data transmission performance of 53.125 Gbaud.

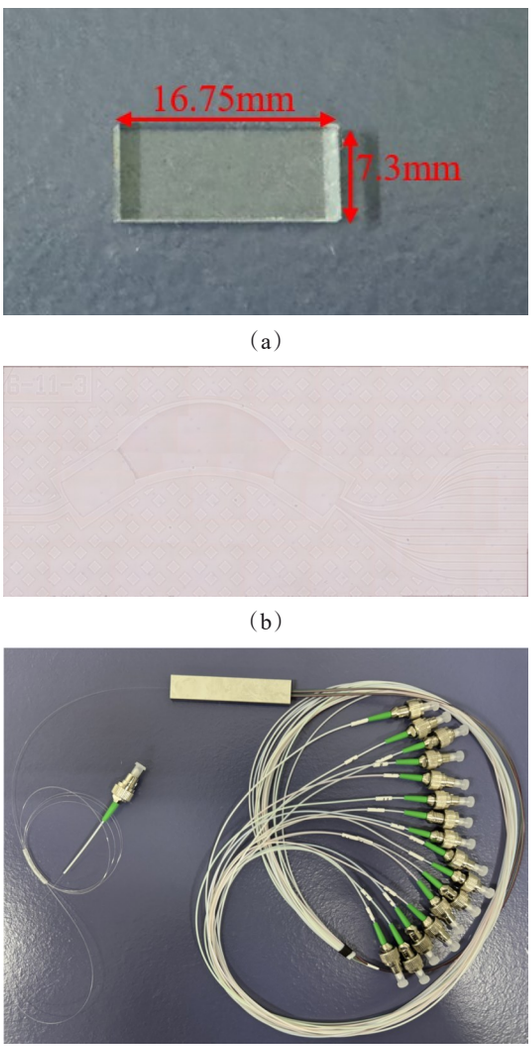

Fig. 8 (a) The photograph of the manufactured AWG chip; (b) the microscope image of the manufactured AWG chip, and (c) the photograph of the packaged 16-channel AWG module
图8 (a)制造好的AWG芯片的照片;(b)制造好的AWG芯片的显微镜图像;(c)封装好的16通道AWG模块的照片

We conduct eye diagram testing on all channels of the AWG for PAM-4 signals. We use an arbitrary waveform generator to generate a 53.125 Gbaud PAM4 signal, which is modulated through an electro-optical modulator onto the optical signal emitted from the tunable laser. The optical signal is then input to the AWG and an oscilloscope is used to capture an eye diagram of the output optical signal from all channels of the AWG. The eye diagrams at standard wavelengths obtained from the test are shown in Fig. 11. We can observe clear eye diagrams, which show that AWG can achieve a total signal rate of 1.6 Tbps, and is expected to achieve even higher rates if we continue to increase the transmission rate of a single channel.

3 Conclusion

We have successfully designed and fabricated an O-band 16-channel AWG with 800 GHz channel spacing

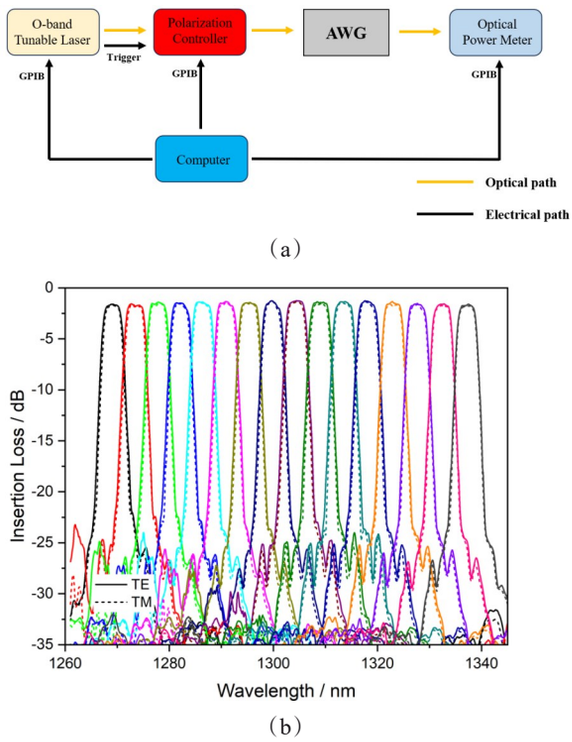

Fig. 9 (a) The experimental setup for testing spectral response; (b) The measured spectral response.
图九 (a)测试光谱响应的实验装置图;(b)测得的光谱响应图

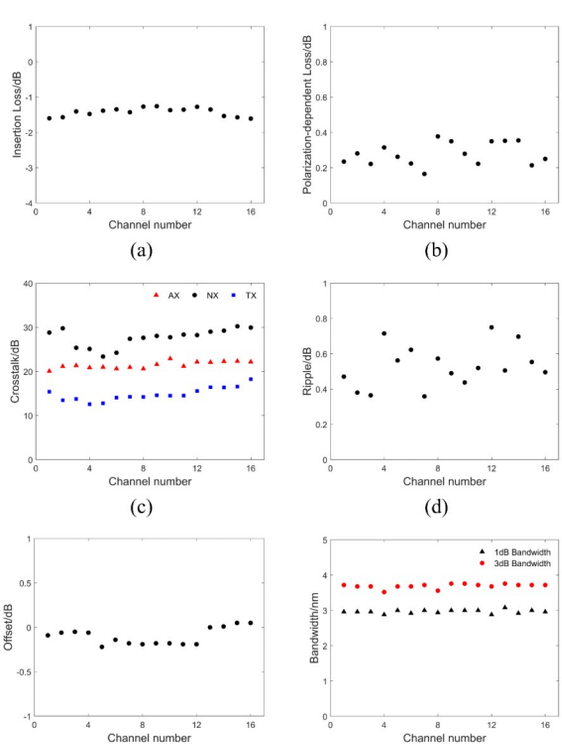

Fig. 10 (a) insertion loss for each channel; (b) polarization-dependent loss; (c) crosstalk; (d) ripple; (e) offset; (f) bandwidth
图10 (a)各通道的插入损耗;(b)偏振相关损耗;(c)串扰;(d)纹波;(e)中心波长偏移;(f)带宽

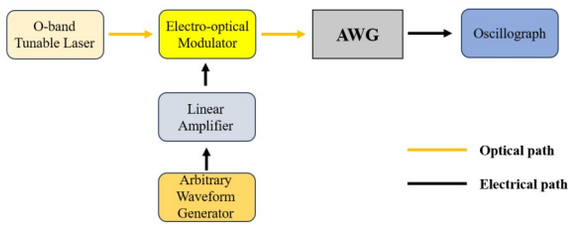

(a)

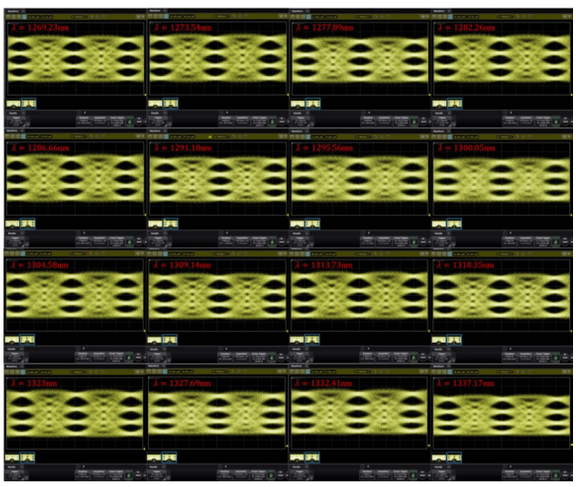

(b)

Fig. 11　(a) Experimental setup for testing eye diagrams and (b) the measured 53.125 GBaud PAM4 optical eye diagrams for all channels: 图十一 (a)测试眼图的实验装置图(b)所有通道的 53.125 GBaud PAM4 光眼图测量结果

based on an ultra-high refractive index difference of 2% silica PLC platform. The transitions between the arrayed waveguides and the slab waveguides are designed as tapered structures, optimizing the insertion loss to be under -1.61 dB, loss uniformity below 0.35 dB. The output waveguides are widened into multimode waveguides to improve the flatness of the output spectrum, resulting in a 1 dB bandwidth greater than 2.88 nm and maintaining crosstalk below -20.05 dB. At the same time, PDL is below 0.35 dB, the center wavelength offset is under 0.22 nm, and the ripple is less than 0.75 dB. We further validate that the AWG is capable of transmitting 53.125 GBaud PAM4 signal per channel, making it suitable for use in 1.6T data center networks. This design provides low insertion loss, low crosstalk, polarization insensitivity and high uniformity, making it highly suitable for optical modules in data centers, enabling signal transmission rates of 1.6 Tbps and above.

References

[1] J. Zou, F. Sun, C. Wang, et al. Silicon-Based Arrayed waveguide gratings for WDM and spectroscopic analysis applications, Opt. Laser Technol. 147 (2022).

[2] F. Horst, W.M. Green, S. Assefa , et al. Cascaded Mach-Zehnder wavelength filters in silicon photonics for low loss and flat pass-band WDM (de-) multiplexing, Opt Express 21 (10) (2013) 11652 - 11658

[3] P. Pan, J. An, Y. Wang , et al. Compact 4-channel AWGs for CWDM and LAN WDM in data center monolithic applications, Opt. Laser Technol. 75 (2015) 177 - 181.

[4] YUAN Pei, WANG Yue, WU Yuan-Da, et al. 25-channel 200 GHz AWG based on SOI ridge waveguides[J]. Journal of Infrared and Millimeter Waves, 2018, 37(6): 673~678

[5] FANG Qing, LI Fang, LIU Yu-Liang. FABRICATION OF ARRAYED WAVEGUIDE GRATING BASED ON SOI MATERIAL[J]. Journal of Infrared and Millimeter Waves, 2005, 24(2): 143~146..
方青, 李芳, 刘育梁. 基于SOI材料的阵列波导光栅的制作[J]. 红外与毫米波学报, 2005, 24(2): 143~146

[6] T. Yoshimatsu, M. Nada, M. Oguma, et al. Compact and high-sensitivity 100-Gb/s (4 × 25 Gb/s) APD-ROSA with a LAN-WDM PLC demultiplexer, Opt. Express 20 (26) (2012) B393 - B398.

[7] Y. Doi, Y. Nakanishi, T. Yoshimatsu, et al. Compact 8-wavelength receiver optical sub-assembly with a low-loss AWG demultiplexer for 400-gigabit datacom, 2015 European Conference on Optical Communication (ECOC) (2015) 1 - 3.

[8] C. Ferrari, C. Bolle, M.A. Cappuzzo, et al. Compact hybrid-integrated 400 Gbit/s WDM receiver for short-reach optical interconnect in datacenters, 2014 The European Conference on Optical Communication (ECOC) (2014) 1 - 3.

[9] Lei Liu, Limin Chang, Yingxin Kuang, et al. "Low-cost hybrid integrated 4 × 25 GBaud PAM-4 CWDM ROSA with a PLC-based arrayed waveguide grating de-multiplexer," Photon. Res. 7, 722-727 (2019)

[10] Seok-Jun Yun, Young-Tak Han, Seok-Tae Kim, et al. "Compact Hybrid-Integrated 4 × 80-Gbps TROSA Module Using Optical Butt-Coupling of DML/SI-PD and Silica AWG Chips," J. Lightwave Technol. 39, 2468-2475 (2021)

[11] Pengwei Cui, Yue Wang, Liangliang Wang, et al. Silica-Based Hybrid-Integrated Receiver Optical Subassembly for 400 Gbps Ethernet, Optics & Laser Technology.

[12] T. Wettlin, S. Ohlendorf, T. Rahman, et al. "Beyond 200 Gb/s PAM4 transmission using Tomlinson-Harashima precoding," 45th European Conference on Optical Communication (ECOC 2019), Dublin, Ireland, 2019

[13] X. Pang, O. Ozolins, R. Lin, et al. "200 Gbps/Lane IM/DD Technologies for Short Reach Optical Interconnects," in Journal of Lightwave Technology, vol. 38, no. 2, pp. 492-503, 15 Jan.15, 2020

[14] L. Zhang, Y. Sun, X. Qin, et al. "3.2T/6.4T CWDM ROSA for Co-Packaged Optic Transceiver," 2021 Optical Fiber Communications Conference and Exhibition (OFC), San Francisco, CA, USA, 2021, pp. 1-3.

[15] Y. Sakamaki, S. Kamei, T. Hashimoto, et al. "Loss Uniformity Improvement of Arrayed-Waveguide Grating With Mode-Field Converters Designed by Wavefront Matching Method," in Journal of Lightwave Technology, vol. 27, no. 24, pp. 5710-5715, Dec.15, 2009, doi: 10.1109/JLT.2009.2034030.

[16] Ye T, Fu Y, Qiao L, et al. Low-crosstalk Si arrayed waveguide grating with parabolic tapers [J]. Opt Express, 2014, 22 (26): 31899-906.